

Neutron star properties in the Thomas-Fermi model

K. Strobel^{a,*}, F. Weber^{a,†}, M. K. Weigel^b,
and Ch. Schaab^a

^a Institut für Theoretische Physik, Universität München
Theresienstrasse 37, D-80333 München, Germany

^b Sektion Physik, Universität München
Am Coulombwall 1, D-85748 Garching, Germany

August 6, 2018

Abstract

The modern nucleon-nucleon interaction of Myers and Swiatecki, adjusted to the properties of finite nuclei, the parameters of the mass formula, and the behavior of the optical potential is used to calculate the properties of β -equilibrated neutron star matter, and to study the impact of this equation of state on the properties of (rapidly rotating) neutron stars and their cooling behavior. The results are in excellent agreement with the outcome of calculations performed for a broad collection of sophisticated nonrelativistic as well as relativistic models for the equation of state.

PACS: numbers: 21.65.+f, 21.30.+y, 97.60.Jd

LBNL-39604

*e-mail: kstrobel@gsm.sue.physik.uni-muenchen.de

†Present address (until 31 December 1996): Lawrence Berkeley National Laboratory, Nuclear Science Division, MS 70A - 3307, Berkeley, CA 94720, USA

I Introduction

The equation of state (EOS) of dense nuclear matter plays a decisive role in many branches of physics. It is an important input quantity for the understanding of heavy-ion collisions, supernova explosions, and the structure of neutron stars [1]-[5]. Therefore great efforts have been made by several groups to derive the EOS of such matter. These models can be divided into two categories, namely nonrelativistic potential models and relativistic, field-theoretical ones. A frequently used model that belongs to the first category is the Skyrme Hamiltonian which has the advantage, being a phenomenological approach, to reproduce the nuclear data rather well. Extensive calculations of neutron star matter properties for this scheme have been performed (see, for instance, Refs. [4, 6, 7]). More elaborate, microscopic schemes constitute the nonrelativistic potential models, where one uses realistic nucleon-nucleon potentials in combination with sophisticated many-body approximations. A typical example of this kind is the work of Wiringa et al. [8], in which the properties of matter were calculated for a Hamiltonian containing two- and three-body interactions. These extensive calculations with some later refinements are still the basis for the calculation of neutron star properties (in the nonrelativistic approach) in several investigations [9]. The disadvantage of such a microscopic treatment is the numerical complexity of the method. For that reason it is very tempting to use simpler models which are easier to deal with, and make comparisons with respect to the properties of finite nuclei, the parameters of the mass formula, and neutron stars. For this purpose we selected the new Thomas-Fermi approach (TF) of Myers and Swiatecki [10], where the density- and momentum dependent interaction is given by [the upper (lower) sign corresponds to nucleons with equal (unequal) isospin]:

$$v_{12\tau} = -\frac{2T_{0\tau}}{\rho_0} f\left(\frac{r_{12}}{a}\right) \times \left(\frac{1}{2}(1 \mp \xi)\alpha - \frac{1}{2}(1 \mp \zeta) \left(\beta \left(\frac{p_{12}}{p_0} \right)^2 - \gamma \frac{p_0}{|p_{12}|} + \sigma \left(\frac{2\bar{\rho}}{\rho_0} \right)^{\frac{2}{3}} \right) \right). \quad (\text{I.1})$$

The quantities ρ_0 , p_0 , and $T_{0\tau} (= p_0^2/2m_\tau)$ denote the baryon number density, Fermi momentum, and the kinetic single-particle energy of symmetric nuclear matter at saturation, respectively. The potential's radial dependence, f , is chosen to be Yukawa type. The choice $\xi \neq \zeta$ leads to a better description

of asymmetric nuclear systems, and the behavior of the optical potentials is improved by the term $\sigma(2\bar{\rho}/\rho_0)^{2/3}$, where $\bar{\rho}^{2/3} = 0.5(\rho_1^{2/3} + \rho_2^{2/3})$. As discussed in great detail by Myers and Swiatecki, this model (with only seven free parameters) has the advantage over the former Seyler–Blanchard interaction [11, 12] to not only reproduce the ground–state properties of finite nuclei and symmetric infinite nuclear matter but also the optical potential and, as revealed by a comparison with the theoretical investigations of Friedman and Pandharipande [13], the properties of pure neutron matter, too. Therefore we think this approximation, which is able to account for so many features in a very satisfying fashion, constitutes, despite its simplicity, an excellent candidate for the investigation of dense matter in the nonrelativistic approach (see also [14] where a simpler force has been used). Since the standard comparison with nuclear physics quantities has already been performed by Myers and Swiatecki [10], we will concentrate in this contribution on the properties of neutron star matter and the structure and thermal evolution of neutron stars constructed for their model. The outcome will be compared with the one obtained for a broad collection of other models for the equation of state, which comprises nonrelativistic potential models as well as relativistic, field-theoretical ones. We shall not go into details concerning these models, whose properties have been discussed in numerous investigations prior to this one (see, for instance, Refs. [3, 4, 5] and [15]–[21]).

II Equation of State

a Symmetric and Asymmetric Nuclear Matter

The explicit expressions for the energy per baryon, E/A , chemical potentials, μ , pressure, P , effective masses, m^* , and symmetry energy J are given in Refs. [10, 22] and will not be repeated here again. For the parameters of the TF model of Myers and Swiatecki we use the most recent set denoted TF [23] (We denote the different parameter sets with TF90, TF94, and TF96. If not stated otherwise the latest parametrization, TF96 (\equiv TF), is used.). Earlier parametrizations (TF90, TF94) have larger statistical errors in fitting the nuclear data. The EOSs for the parameter sets of Ref. [23] are rather similar, but the EOS for the parameter set TF90 of Ref. [10] is stiffer than the latter EOSs (see Table I). For the purpose of comparison, we give the

parameters of symmetric infinite nuclear matter for the different models in Table I. (An overview of all EOSs used in this work is given in Table II).

Nonrelativistic Brueckner–Hartree–Fock calculations (BHF) with two–body forces are in general not capable to reproduce the correct saturation properties. The resulting EOSs are too soft. This deficiency is corrected by adding three–body forces (TBF) which lead to improved saturation properties and a stiffer EOS. Nevertheless the BHF calculations occur to be not satisfactory enough for the description of symmetric infinite nuclear matter (see Refs. [8, 9] and Table I) and we will therefore not discuss them in greater detail. Stiffer EOSs are also obtained in the Dirac–Brueckner–Hartree–Fock approach (DBHF) [21],[24]–[28]. The general trend seems to be that variational calculations, BHF supplemented with TBF, and DBHF calculations agree with each other more or less only up to moderate densities. At higher densities one obtains a closer agreement of DBHF with the variational calculations, depending on the matter’s asymmetry [8, 9, 25, 26]. Our main intention is to discuss the properties of the EOS of neutron star matter, and compare the results with those obtained in the nonrelativistic many–body approach as well as the fieldtheoretical treatment. As examples belonging to the first category, we have selected EOSs from the investigations of Wiringa et al. [8], which have been used frequently in neutron star calculations by others, too. The two samples are (cf. Table II) the variationally–based EOSs computed for the Urbana UV14 two–nucleon potential supplemented with the UVII three–nucleon potential (WUU), and the density–dependent UV14 potential supplemented with the three–nucleon interaction TNI (WUT). As representatives of the DBHF and relativistic Hartree–Fock (RHF) scheme we have chosen EOSs from Refs. [19, 21, 24, 26].

As pointed out above, the DBHF–EOSs are stiffer than BHF–EOSs based on two–body forces, but by introducing three–body forces one can simulate the relativistic behavior to a certain extent [8, 9]. In Fig. 1 we illustrate the situation for symmetric nuclear matter. The agreement of all models, with the exception of the BHF model based on two–body forces [8, 9, 26, 28], is better than in the case of pure neutron matter (see Figs. 2 and 3), where larger deviations occur above $\rho = 0.4 \text{ fm}^{-3}$. The potential model of Myers and Swiatecki leads to a pure neutron–matter EOS which is located between the two nonrelativistic variational calculations WUU and WUT. The larger differences between nonrelativistic and relativistic models for higher asym-

metry are explainable by the different behavior of the symmetry energy. The nonrelativistic potential models cause a stronger repulsion in isospin singlet states for higher densities [8], which makes for increasing asymmetry the nonrelativistic EOSs softer in comparison with the relativistic ones. This behavior can be clearly seen in the density dependence of the symmetry energy (see Fig. 4), where TF shows a similar behavior as WUT. It seems to be a general feature that relativistic treatments lead to a monotonic increase of the symmetry energy, in contrast to the nonrelativistic models where the symmetry energy saturates (for BHF [8, 9, 26]), or even decreases with increasing density (variational calculations). As we shall discuss later, this feature has a severe impact on the composition of neutron star matter, since the symmetry energy determines the proton fraction of neutron star matter. The proton fraction in turn plays an important role for the cooling behavior of neutron stars, since proton fractions above $\sim 0.11 - 0.13$ permit stars to cool very efficiently via the direct Urca process [29, 30].

b Neutron Star Matter

Since neutron stars are bound by gravity, which is much weaker than the Coulomb force, and have life times practically infinite compared to the characteristic weak interaction time scale, $\tau_w \sim 10^{-10}$ s, neutron star matter is subject to the constraints of charge neutrality and generalized β -equilibrium, respectively [2, 3, 4, 8, 18, 22]:

$$\sum_{B=p,n} q_B (2J_B + 1) \frac{k_{F,B}^3}{\pi^2} - \sum_{L=e,\mu} \frac{k_{F,L}^3}{3\pi^2} = 0 , \quad (\text{II.2})$$

and

$$\mu_B = \mu_n - q_B \mu_L , \quad \mu_\mu = \mu_e . \quad (\text{II.3})$$

Here $\mu_B(q_B)$ denotes the chemical potentials (electric charges) of baryons, and μ_L the chemical potentials of leptons e^- , μ^- . Due to these constraints the calculation of neutron-star-matter properties differs from the treatment of asymmetric matter, since the composition has to be determined selfconsistently subject to the two additional constraints (II.2) and (II.3). The new baryon/lepton degrees of freedom lower the energy and pressure of neutron star matter in comparison with pure neutron matter [3, 4, 18, 19, 28, 31].

This feature is illustrated in Fig. 5, where the pressure of neutron star matter is shown as function of density and compared with the pressure of pure neutron matter. Due to the new degrees of freedom, the pressure is lower in β -stable matter. To demonstrate the influence of muons on the EOS, we also show the EOS computed for n , p , and e^- only. It indicates that the muons play only a minor role for the stiffness of the EOS. Nevertheless they are important for the composition. For the neutron star matter EOS computed for the model of Myers and Swiatecki one does expect deviations from the microscopic calculations which are of the same order as for the calculations performed for fixed asymmetry.

In Figs. 6 and 7 we show the energy per baryon of neutron star matter for the different models. The nonrelativistic models give in general softer EOSs, but the model of Myers and Swiatecki comes rather close to the relativistic results (HWW1), especially at lower densities. The earlier parametrization of Myers and Swiatecki, that is TF 90, comes even closer to the relativistic outcome [22], since the EOS is much stiffer.

The same behavior holds also for the pressure, which is exhibited in Fig. 8. Much larger differences than for the EOS occur for the composition of neutron stars [22]. Due to the behavior of the symmetry energy discussed above, one encounters in relativistic models a monotonous increase of the proton fraction, x ($\equiv \rho_p/\rho$) with density (in the case of no hyperons and/or meson condensates), in contrast to nonrelativistic microscopic theories and the TF model of Myers and Swiatecki for which x decreases (or saturates as for BHF) at higher densities. This is illustrated in Fig. 9 and Table III, where the composition is compared for several different models. In this context we note that the stiffness of modern fieldtheoretical models which – besides neutrons and protons account for the population of more massive baryon states (especially hyperons) too – comes closer to the stiffness one of nonrelativistic neutron star matter EOSs [3, 18, 19, 31]. Here one obtains again a decrease of the electron/muon fraction, since it is energetically favorable for the system to achieve charge neutrality among the hyperons themselves.

III Neutron Star Properties

In order to determine neutron star properties one has to solve Einstein's equations, for which knowledge of the EOS, i.e. $P(\epsilon)$, is necessary. Einstein's

curvature tensor $G_{\mu\nu}$ ($R_{\mu\nu}$, $g_{\mu\nu}$, R , and $T_{\mu\nu}$ denote the Ricci tensor, metric tensor, Ricci scalar, and energy–momentum tensor density, respectively) is determined by

$$G_{\mu\nu} \equiv R_{\mu\nu} - \frac{1}{2} g_{\mu\nu} R = 8\pi T_{\mu\nu}(\epsilon, P(\epsilon)) . \quad (\text{III.4})$$

For the determination of the properties of (rapidly) rotating neutron stars and their limiting periods, one has to generalize the Schwarzschild metric of a spherically symmetric, static star to the one of a rotationally deformed, axially symmetric body [32, 33]:

$$ds^2 = e^{-2\nu(r,\theta;\Omega)} dt^2 + e^{2\psi(r,\theta;\Omega)} (d\phi - \omega(r,\theta;\Omega) dt)^2 + e^{2\mu(r,\theta;\Omega)} d\theta^2 + e^{2\lambda(r,\theta;\Omega)} dr^2 . \quad (\text{III.5})$$

Ω denotes the neutron star’s rotational frequency, and $\omega(r,\theta;\Omega)$ is the angular velocity of the local inertial frames (dragging of the local inertial frames) [3, 32, 34]).

Of great interest with respect to the identification of rapidly spinning pulsars as rotating neutron stars is the maximum possible rotational frequency of such an object, for which no simple stability criteria exist in general relativity. However an absolute upper limit is given by the Kepler frequency, Ω_K , at which mass shedding at the equator sets in. It is determined as the solution of the following transcendental equation [27, 32, 33],

$$\Omega_K = \left\{ e^{\nu(r,\theta;\Omega_K) - \psi(r,\theta;\Omega_K)} V(r,\theta,\Omega_K) + \omega(r,\theta,\Omega_K) \right\}_{\text{eq}} , \quad (\text{III.6})$$

which is to be evaluated at the star’s equator. V denotes the velocity of a particle rotating at the star’s equator. Equations (III.4) and (III.6) are to be solved simultaneously by a selfconsistent numerical iteration scheme, since neither the metric functions in (III.5) nor the frequencies Ω_K and ω (all depend on the star’s unknown mass) are known.

In Fig. 10 we exhibit the neutron star masses as a function of central energy density for different EOSs. Since WUU and WUT behave rather similar up to mass densities of about $\sim 10^{15} \text{g/cm}^3$, the mass-density curves computed for these two EOSs are very similar to each another. The deviations beyond that density arise from the different three–body forces. The TF–EOS behaves for smaller energy densities like the relativistic EOS, but

shows at higher densities features similar to a medium–stiff EOS. So the properties of neutron stars computed for TF and HWW2, which are listed in Tables IV and V, are similar to each other as long as the star’s mass is below about $1.4 M_{\odot}$. Besides HWW2 the EOS of Brockmann and Machleidt [24, 26] has been chosen here as a further representative of a relativistic EOS. The former accounts for the presence of hyperons in neutron star matter too [27, 31]. The stiffness of an EOS at high densities is known to play a key role for the maximum possible mass that a neutron star can have. Since the non-relativistic EOSs tend to be less stiff at high densities than their relativistic counterparts (the only exception is WUU), we obtain less massive neutron stars for the nonrelativistic EOSs.

Another effect caused by the stiffness of an EOS concerns the radius of the stellar configurations. In general, the stiffer the EOS the lower the star’s central mass density and thus the lower the gravitational force that pulls the star together. So stars constructed for stiffer EOSs will have larger radii than those constructed for softer EOSs. This behavior is confirmed in Fig. 11, where the radius–mass relations of neutron stars constructed for TF and HWW2 are shown: the stiffer model for the EOS, that is HWW2, leads to somewhat bigger stars, provided their mass is beyond about one solar mass. The masses of stars lighter than this value are determined by the stiffness/softness of the EOS at nuclear and intermediate densities where TF behaves stiffer than HWW2, leading to neutron stars that are somewhat bigger for TF than for HWW2. The radial changes due to rotation at Ω_K amount about 2 km, except for the very light stars of each sequence. The mass increase of the heaviest stars due to rapid rotation is about $0.3 M_{\odot}$ (see also Fig. 12). Various properties of static as well as rotating neutron stars, computed for a number of different EOSs, are listed in Tables VI–VIII. All properties refer to neutron stars of mass $M = 1.4 M_{\odot}$ (static and rotating), about which the observed masses tend to scatter.

In Fig. 13 we show the density profiles of nonrotating neutron stars of mass $M = 1.4 M_{\odot}$, which reflect what has just been discussed above in connection with the dependence of stellar radii on the stiffness/softness of the EOS: The microscopic EOSs WUU and WUT, behaving somewhat softer than TF and HWW2, lead to smaller stars with a higher central density (for more phenomenological relativistic EOSs, see Ref. [35]). Moreover, as can be inferred from Fig. 13, the TF–EOS density profile is rather close to the

one of the relativistic HWW2–EOS because of the rather similar behavior of these EOSs over the energy densities relevant for a star of this mass.

A final remark concerns the velocity of sound, which does not exceed the causal limit in the TF model for the range of relevant neutron star densities, i.e., $c_s \leq 0.96 c$ for $\rho \leq 1.246 \text{ fm}^{-3}$. The causal limit is reached at $\rho = 1.36 \text{ fm}^{-3}$, which is considerably higher than the highest density reached in the most massive star of the sequence.

As mentioned above, the Kepler frequency gives an absolute upper limit on the critical rotational frequency of a neutron star. Its rotation may also be limited by the gravitational radiation–reaction instability. Since the theory of this effect is too lengthy, we will not outline the treatment in this investigation but refer to [3, 34, 36] for details. In Fig. 14 we exhibit the limiting rotational periods set by both the Kepler criterion and the gravitational radiation–reaction instability. The latter depend on temperature, for which we have chosen representative values of $T = 10^6 \text{ K}$, corresponding to an old neutron star, and 10^{10} K typical for a young newly formed one. The limiting periods set by the gravitation–radiation instability are larger than the Kepler periods and thus set a more stringent limit on rapid rotation than mass shedding. Moreover they increase with temperature, since viscosity damps the instability modes less efficiently in hot stars. A comparison between TF and HWW2 shows that the differences in rotational periods are rather small, except for hot neutron stars where somewhat larger deviations show up. The shaded rectangle in Fig. 14 covers masses and periods of observed pulsars [37]. Hence both EOSs, based on the assumption that neutron star matter is made up of hadrons and leptons rather than other kinds of exotic forms of matter [3], are in accordance with the body of presently existing data.

A further important facet of neutron star physics concerns the cooling behavior of such objects. In Ref. [35] we have already calculated and discussed in great detail their cooling behavior for different EOSs depending on the involved processes (see, for instance, Table 5 of Ref. [35]). Here we show and compare the cooling tracks of different neutron star models of mass $M = 1.4 M_\odot$. The underlying EOSs are the nonrelativistic TF and WUU models, and the relativistic HWW2. As an example of an enhanced neutrino emission process we consider the direct Urca process, which is only possible if the proton fraction exceeds a certain critical value (≈ 0.13 , see Refs. [29, 30]). Among the considered EOSs, only HWW2 allows for the direct

Urca process. This leads to a large drop of the star’s surface temperature at $\tau \approx 30$ yr (see the dashed curve of the nonsuperfluid model in Fig. 15), since the core cools down very fast via the enhanced neutrino emission process in comparison with the crust, causing a temperature inversion in young stars. Depending on the crust thickness, the cooling wave formed by the temperature gradient reaches the surface and causes the sharp decrease of the surface temperature, followed by a rather flat behavior of the cooling tracks up to 10^7 years [35, 38]. We show also the behavior of superfluid neutron stars. Superfluidity reduces the neutrino emissivity, the heat capacity, and the thermal conductivity by an exponential factor of $\exp(-\Delta/kT)$, where Δ denotes the gap energy (see Table 4 of Ref. [35] for the used gap energies).

The observational data are described in Ref. [39] (see Table IX). The obtained effective surface temperature depends crucially on whether a hydrogen atmosphere is used or not. Since the photon flux, measured solely in the X-ray energy band, does not allow to determine what atmosphere one should use, we consider both the blackbody model (solid error bars in Fig. 15) and the hydrogen-atmosphere model (dashed error bars). The plotted errors represent the 3σ error range due to the small photon fluxes. The pulsars ages are determined by their spin-down times assuming a canonical value of 3 for the braking index. In reality the braking index may be quite different from 3. Its variation between 2 and 4, for instance, would change the age of Geminga as indicated by the horizontal error bar shown at the bottom of Fig. 15.

The cooling tracks of the nonrelativistic models, that is TF and WUU, are almost identical. Since the relativistic HWW2 model cools mainly through the direct Urca process in the neutrino cooling era, its cooling behavior differs considerably from the nonrelativistic models. Superfluidity reduces the neutrino emissivity which leads to a higher surface temperature in the neutrino cooling era. Later, in the photon cooling era, the surface temperature becomes smaller for the superfluid models. The observational data can almost perfectly be described by both the nonsuperfluid and the superfluid nonrelativistic models as well as the superfluid relativistic model, provided one assumes that the pulsars have no hydrogen atmosphere (except PSR 1055-52, which could be explained by internal heating; see, e.g., Refs. [40, 41]). However, if some of the pulsars prove to have a hydrogen atmosphere, these models seem to be too hot. In this case superfluid enhanced cooling or inter-

mediate cooling [38] might be necessary. Whether the observed pulsars have a hydrogen atmosphere could be decided if one considers multiwavelength observations, as suggested by Pavlov et al. [42].

IV DISCUSSION AND CONCLUSIONS

We have calculated within the modern nonrelativistic TF model of Myers and Swiatecki the properties of neutron star matter and compared the outcome with microscopic nonrelativistic and relativistic treatments. The main purpose of this contribution was to test this model with respect to its implications for the physics of neutron stars. It turned out that, despite its simplicity, the modern TF model shows the same features with respect to the EOS of neutron star matter as complicated nonrelativistic variational calculations. Moreover the model is in even closer, over the relevant density regions encountered in neutron stars, with microscopic relativistic EOSs. The composition of neutron star matter obtained for TF is similar to other nonrelativistic models for which the symmetry energy saturates or even decreases at higher densities too, favoring so, in contrast to relativistic models, again an increase of the neutron fraction at higher densities. The resulting gross structural properties of neutron stars (masses, redshifts etc.) are in accordance with observations. Also interesting is the finding that the limiting rotational neutron star periods computed for TF, set by either the Kepler criterion or the gravitational–radiation reaction instability, agree rather closely with the results of modern relativistic EOSs. The limiting period of a $M \sim 1.4 M_{\odot}$ neutron star is about 1 ms, which too is in agreement with the present observations. Limiting periods of this size seem to be a general feature of EOSs computed hadronic/leptonic matter [3, 27]. Finally we studied the thermal evolution of neutron stars for TF. Here, somehow surprisingly, it turned out that no enhanced cooling mechanism needs to be invoked to achieve agreement between theory and observation; cooling via only the modified Urca process occurs to be sufficient. (We recall that cooling via the direct Urca process is not permitted for TF, as is the case for the nonrelativistic microscopic neutron star matter EOSs studied in this work.)

From these findings we conclude that the modern Thomas–Fermi model of Myers and Swiatecki is not only very suitable for the description of low–energy nuclear physics but for phenomena in high–density regime too! Our

study reveals that the TF–EOS of neutron star matter shows similar features as sophisticated microscopic nonrelativistic EOSs and, over some density range, comes even close to microscopic relativistic EOSs. The neutron star properties and the cooling behavior derived for TF are in excellent agreement with the body of presently existing data. Due to these surprising features we think that the model of Myers and Swiatecki is also a very good candidate for the nonrelativistic (many–body) treatment of neutron stars and, therefore, should be included in further nonrelativistic investigations in this field. The handling of this model with only seven parameters is relatively simple in comparison with elaborated microscopic schemes, which makes it an ideal candidate for this kind of astrophysical studies.

Acknowledgments:

We would like to thank W. D. Myers and W. J. Swiatecki for clarifying remarks and helpful discussions.

Table captions

TABLE I: Saturation density, ρ_{00} , energy per baryon, E/A , incompressibility, K , and symmetry energy, J , of symmetric infinite nuclear matter for different models. These are TF: Thomas–Fermi model of Myers and Swiatecki [10, 23]; WUU and WUT: variational calculation performed for UV14 plus UVII and UV14 plus TNI, respectively [8, 9]; BHF2 and BHF3: Brueckner–Bethe approximation with two– (AV 14) and three–body forces (AV 14+UVII), respectively [8, 9]; DBHF⁽¹⁾ and DBHF⁽²⁾: relativistic Dirac–Brueckner–Hartree-Fock approximation with solutions in the space of positive energy–spinors only [24] and the full Dirac space [21], respectively (A and B denote different Brockmann–Machleidt potentials [21, 24]); NL1 and NL–SH: phenomenological relativistic mean field theory for the parameter sets of Reinhard and Sharma, respectively [21]); SKM* and SIII: Skyrme forces [43].

TABLE II: Equations of state (EOSs) used in this work.

TABLE III: Proton fraction, x , and energy per baryon (in MeV) of beta–stable matter (neutrons, protons, electrons and muons).

TABLE IV: Neutron star properties for beta–stable TF model (neutrons, protons, electrons and muons). $M_G(\epsilon_c)$ denotes the gravitational mass in solar mass units as a function of central mass density. The central star pressure is denoted p_c . The amu mass M_A minus the gravitational mass M_G is effectively the binding energy liberated when the NS is formed. R stands for the star’s radius, Δ_c denotes the stellar crust using 2.4×10^{14} g cm^{−3} as the boundary, I denotes the moment of inertia, and z the surface redshift. For a comparison with WUU and WUT see Ref. [8].

TABLE V: Same as Table IV, but for the HWW2 model.

TABLE VI: Comparison of the properties of a static, spherical NS of mass $1.4 M_\odot$ for different models.

TABLE VII: Properties of rotating neutron star models of mass $M = 1.4 M_\odot$ and rotational period $P = 1$ ms, calculated for different EOSs.

The entries are (from top to bottom): central energy density, ϵ_c ; percental mass increase relative to nonrotating star model of same ϵ_c , $\Delta M/M$; equatorial and polar radii, R_{eq} and R_{p} , respectively; moment of inertia, I ; stability parameter, t ; injection energy, β ; redshift at the pole, z_{p} ; eccentricity, e ; quadrupole moment, Π . The influence of different parametrizations of the TF model on NS properties is shown too. The stiffness of the TF EOSs decreases from TF90n (pure neutron matter, represents the stiffest EOS) to TF96.

TABLE VIII: Same as Table VII, but for a rotational period of $P = 1.6$ ms.

TABLE IX: Surface temperatures, T_s^∞ , and spin-down ages, t , of several observed pulsars [35, 38, 39].

TABLE I

Method	E/A (MeV)	ρ_{00} (fm ⁻³)	K (MeV)	J (MeV)
TF90	-16.53	0.165	301	32
TF94	-16.04	0.161	234	32
TF96	-16.24	0.161	234	33
WUU	-15.5	0.175	202	30
WUT ^{a)}	-16.6	0.157	261	29
BHF 2	-17.8	0.280	247	–
BHF 3	-15.2	0.194	209	–
DBHF A ⁽¹⁾	-15.6	0.185	290	–
DBHF A ⁽²⁾	-16.5	0.174	280	34
DBHF B ⁽¹⁾	-13.6	0.174	249	–
DBHF B ⁽²⁾	-15.7	0.172	249	33
NL 1	-16.4	0.152	212	43
NL-SH	-16.3	0.146	356	36
SkM*	-15.8	0.160	216	30
SIII	-15.9	0.145	355	28
a) in Ref. [26]:	-15.7	0.158	246	

TABLE II

EOS	Interaction	Many-body approach	Ref.
TF90	Myers and Swiatecki	Thomas-Fermi	[10, 22]
TF94	Myers and Swiatecki	Thomas-Fermi	[23]
TF96	Myers and Swiatecki	Thomas-Fermi	[23]
WUU	Urbana 2-nucleon potential UV14 plus Urbana 3-nucleon potential UVII	variational	[8]
WUT	Urbana 2-nucleon potential UV14 Urbana 3-nucleon potential TNI	variational	[8]
BHF2	Argonne 2-nucleon potential AV14	nonrelativistic Brueckner-Bethe	[8, 9]
BHF3	Argonne 2-nucleon potential AV14 plus Urbana 3-nucleon potential UVII	nonrelativistic Brueckner-Bethe	[8, 9]
RB	Brockmann-Machleidt potential A	relativistic Brueckner- Hartree-Fock	[24, 26]
HWW1	Brockmann-Machleidt potential A (no hyperons)	relativistic Brueckner- Hartree-Fock	[28]
HWW2	Brockmann-Machleidt potential B + HFV	relativistic Brueckner- Hartree-Fock	[27, 31]
HV	Exchange of σ , ω and ρ mesons (with hyperons)	relativistic Hartree	[3]
HFV	Exchange of σ , ω and ρ mesons (with hyperons)	relativistic Hartree-Fock	[3]

TABLE III

ρ (fm ⁻³)	TF		WUU		WUT	
	$x(\rho)$	$E(\rho, x)$	$x(\rho)$	$E(\rho, x)$	$x(\rho)$	$E(\rho, x)$
0.07	0.0276	5.88	0.0193	8.13	0.0247	6.25
0.08	0.0308	6.25	0.0213	8.66	0.0273	6.43
0.10	0.0365	7.05	0.0253	9.70	0.0317	6.87
0.125	0.0427	8.25	0.0300	11.06	0.0357	7.69
0.15	0.0502	9.48	0.0345	12.59	0.0388	8.89
0.175	0.0572	10.97	0.0402	14.18	0.0418	10.32
0.20	0.0630	12.83	0.0464	15.92	0.0442	12.13
0.25	0.0715	17.78	0.0572	20.25	0.0469	16.76
0.30	0.0767	24.36	0.0632	25.78	0.0476	22.53
0.35	0.0794	32.57	0.0673	32.60	0.0476	29.18
0.40	0.0803	42.34	0.0741	40.72	0.0472	36.75
0.50	0.0780	66.28	0.0854	61.95	0.0401	56.06
0.60	0.0725	95.56	0.0959	90.20	0.0311	79.19
0.70	0.0651	129.62	0.1108	126.20	0.0195	106.04
0.80	0.0572	167.97	0.1215	170.50	0.0054	135.46
1.00	0.0417	256.15	0.1239	291.10	4.8e-4	200.89
1.25	0.0274	385.57	0.0855	501.00	0.0000	294.00
1.50	0.0152	534.64	0.0195	753.00	0.0000	393.00

TABLE IV

ϵ_c (10^{14}) (g/cm ³)	p_c (10^{34}) (dyn/cm ²)	M_G (M_\odot)	$M_A - M_G$ (M_\odot)	R (km)	Δ_c (km)	I (10^{44}) (g cm ²)	z
2.5	0.2703	0.131	0.001	17.89	16.08	0.569	0.011
3.0	0.4496	0.184	0.003	14.17	9.90	0.854	0.020
3.5	0.7009	0.248	0.005	12.68	7.06	1.26	0.030
4.0	1.046	0.327	0.009	11.99	5.36	1.82	0.043
5.0	2.007	0.504	0.022	11.53	3.54	3.30	0.072
6.0	3.387	0.696	0.041	11.45	2.57	5.15	0.104
7.0	5.218	0.887	0.067	11.45	1.98	7.21	0.139
8.0	7.518	1.07	0.098	11.45	1.59	9.26	0.174
10.0	13.46	1.36	0.163	11.38	1.13	12.9	0.244
12.5	23.28	1.62	0.239	11.19	0.82	16.0	0.322
15.0	35.38	1.78	0.297	10.95	0.64	17.9	0.387
17.5	49.47	1.88	0.339	10.71	0.53	18.7	0.442
20.0	65.27	1.94	0.366	10.47	0.46	18.9	0.487
25.0	101.1	1.99	0.392	10.06	0.37	18.6	0.553
30.0	141.6	2.00	0.396	9.73	0.33	17.9	0.598
35.0	185.6	1.99	0.390	9.43	0.27	17.0	0.633

TABLE V

ϵ_c (10^{14}) (g/cm ³)	p_c (10^{34}) (dyn/cm ²)	M_G (M_\odot)	$M_A - M_G$ (M_\odot)	R (km)	Δ_c (km)	I (10^{44}) (g cm ²)	z
2.5	0.3146	0.144	0.002	14.47	12.44	0.598	0.015
3.0	0.5156	0.212	0.004	12.59	8.03	1.04	0.026
3.5	0.7731	0.282	0.007	11.95	6.11	1.54	0.037
4.0	1.055	0.345	0.010	11.68	5.06	2.02	0.047
5.0	2.218	0.539	0.024	11.37	3.29	3.66	0.078
6.0	3.655	0.735	0.048	11.36	2.41	5.59	0.112
7.0	5.724	0.955	0.085	11.44	1.83	8.09	0.152
8.0	9.006	1.21	0.146	11.52	1.37	11.4	0.204
10.0	17.48	1.61	0.280	11.55	0.91	17.0	0.302
12.5	30.81	1.91	0.423	11.42	0.64	21.5	0.404
15.0	46.21	2.06	0.519	11.20	0.50	23.6	0.481
17.5	61.29	2.13	0.571	11.00	0.43	24.2	0.530
20.0	78.08	2.17	0.602	10.81	0.40	24.2	0.568
25.0	112.3	2.19	0.624	10.45	0.33	23.4	0.619
30.0	148.3	2.18	0.621	10.18	0.31	22.2	0.647
35.0	185.4	2.15	0.609	9.95	0.29	21.1	0.665

TABLE VI

Quantity	TF	WUU	WUT	HW2
$\epsilon_c(10^{14} \text{ g/cm}^3)$	10.30	10.42	12.12	8.9
$P_c(10^{34} \text{ dyn/cm}^2)$	14.54	15.74	18.58	12.37
M_G/M_\odot	1.4	1.4	1.4	1.4
$(M_A - M_G)/M_\odot$	0.173	0.162	0.169	0.203
R (km)	11.37	11.15	10.86	11.56
Δ_c (km)	1.08	1.06	0.88	1.12
$I(10^{44} \text{ g cm}^2)$	13.34	12.80	12.30	13.97
z	0.254	0.261	0.271	0.248

TABLE VII

Quantity	TF90n	TF90	TF94	TF96	HWW2	WUU
ϵ_c (MeV/fm ³)	410.6	430.1	490.3	508.1	451.3	531.2
$\Delta M/M$	17	13	13	13	14	11
R_{eq} (km)	14.50	13.59	12.99	12.82	13.03	12.02
R_p (km)	10.64	10.35	10.21	10.16	10.18	9.82
$\log I$ /(g cm ²)	45.0829	45.0704	45.0568	45.0525	45.0596	45.0345
t	0.082	0.076	0.068	0.066	0.070	0.060
β	0.610	0.600	0.595	0.593	0.594	0.579
z_p	0.2792	0.2905	0.2966	0.2986	0.2979	0.3141
e	0.68	0.65	0.62	0.61	0.62	0.58
Π (km ³)	14.7	12.6	10.4	9.8	11.0	8.1

TABLE VIII

Quantity	TF90n	TF90	TF94	TF96	HWW2	WUU
ϵ_c (MeV/fm ³)	454.0	465.8	531.3	549.9	480.9	560.7
$\Delta M/M$	6	5	5	5	6	4
R_{eq} (km)	13.05	12.47	12.00	11.88	12.07	11.30
R_p (km)	11.74	11.35	11.03	10.94	11.06	10.51
$\log I$ /(g cm ²)	45.1419	45.1275	45.1055	45.0990	45.1155	45.0803
t	0.031	0.029	0.026	0.025	0.027	0.023
β	0.650	0.635	0.625	0.622	0.625	0.606
z_p	0.2425	0.2549	0.2649	0.2679	0.2649	0.2841
e	0.44	0.42	0.39	0.39	0.40	0.37
Π (km ³)	5.5	4.8	3.9	3.7	4.2	3.1

TABLE IX

Pulsar	t [yr]	Model atmosphere	T_s^∞ [K]
0833-45 (Vela)	1.1×10^4	blackbody	1.3×10^6
		magnetic H-atmosphere	$7.0_{-1.3}^{+1.6} \times 10^5$
0656+14	1.1×10^5	blackbody	$7.8_{-4.2}^{+1.5} \times 10^5$
		H-atmosphere	$5.3_{-0.9}^{+1.2} \times 10^5$
0630+18 (Geminga)	3.2×10^5	blackbody	$5.2 \pm 3.0 \times 10^5$
		H-atmosphere	$1.7 \pm 1.0 \times 10^5$
1055-52	5.4×10^5	blackbody	$7.9_{-3.0}^{+1.8} \times 10^5$

Figure captions

- Fig. 1.** EOSs of symmetric infinite nuclear matter. Compared are: TF, WUU and WUT, BHF2, BHF3, RB, and HWW1. (The abbreviations are explained in Table II.)
- Fig. 2.** Comparison of pure neutron matter EOSs.
- Fig. 3.** Enlargement of the EOSs of neutron matter at low densities. Labels as in Fig. 1. The triangles (HWW1) show the results of DBHF-calculations (potential A) performed in the full Dirac space (for details, see Ref. [21, 27, 28]).
- Fig. 4.** Comparison of the symmetry energy in the relativistic and nonrelativistic approaches.
- Fig. 5.** Variation of the EOS with composition in the TF-model. Compared is pressure versus density of neutron star matter, composed of p, n, e^- and μ^- , with the pure neutron matter case. The influence of muons on the EOS is exhibit too.
- Fig. 6.** Comparison of EOSs of β -equilibrated (i.e., n, p, e^- and μ^-) neutron star matter.
- Fig. 7.** High-density behavior of the EOSs of β -stable neutron star matter.
- Fig. 8.** Pressure-density relation of neutron star matter for different models.
- Fig. 9.** Comparison of the proton fractions associated with the various different EOSs studied in this paper.
- Fig. 10.** Gravitational mass of static (nonrotating) neutron star sequences versus central energy density for different neutron star matter EOSs.
- Fig. 11.** Neutron star radius versus mass for TF and the relativistic HWW2-EOS. Shown are sequences of stars rotating at their general relativistic Kepler frequencies, and at zero frequency.
- Fig. 12.** Gravitational neutron star mass versus central star energy density for TF and the relativistic HWW2-EOS. Shown are sequences of stars rotating at their Kepler frequencies, and at zero frequency.

Fig. 13. Mass density profiles of a $1.4 M_{\odot}$ neutron star computed for several different EOSs.

Fig. 14. Limiting rotational periods ($P = 2\pi/\Omega$) of neutron star sequences versus star mass. Shown are the Kepler periods and the limiting periods set by the emission of gravity waves from young neutron stars ($10^{10} K$) as well as old ones ($10^6 K$). The underlying EOSs are TF and the relativistic HWW2. The shaded area covers the range of observed periods and masses (see text).

Fig. 15. Cooling of neutron stars constructed for TF, WUU and HWW2, with and without inclusion of superfluidity. The surface temperatures obtained with a blackbody– (magnetic hydrogen) atmosphere are marked by solid (short–dashed) error bars (see Table IX). The uncertainty in the pulsar’s age is indicated by the error bar in the lower right corner [39].

FIGURE 1

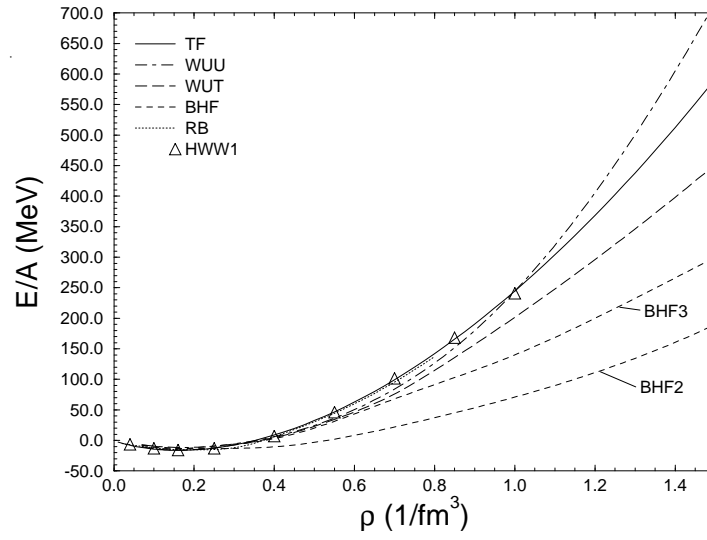


FIGURE 2

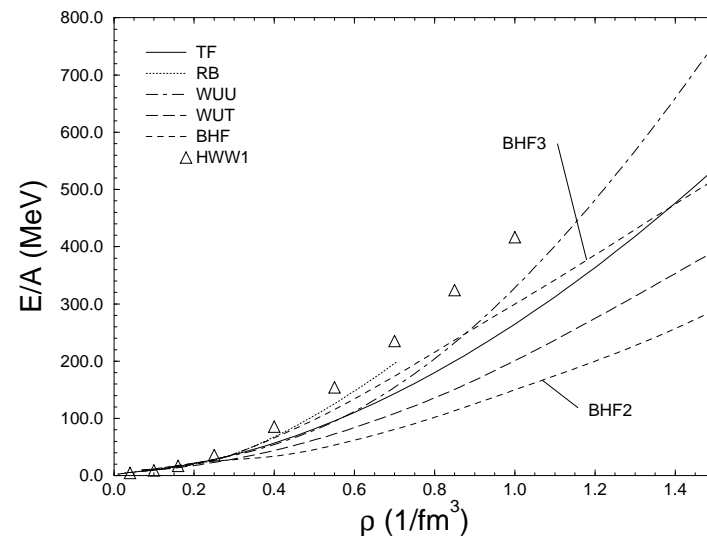


FIGURE 3

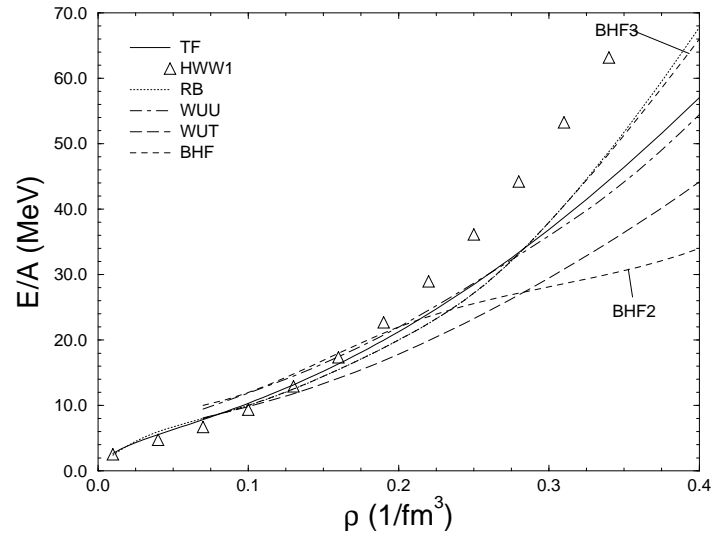


FIGURE 4

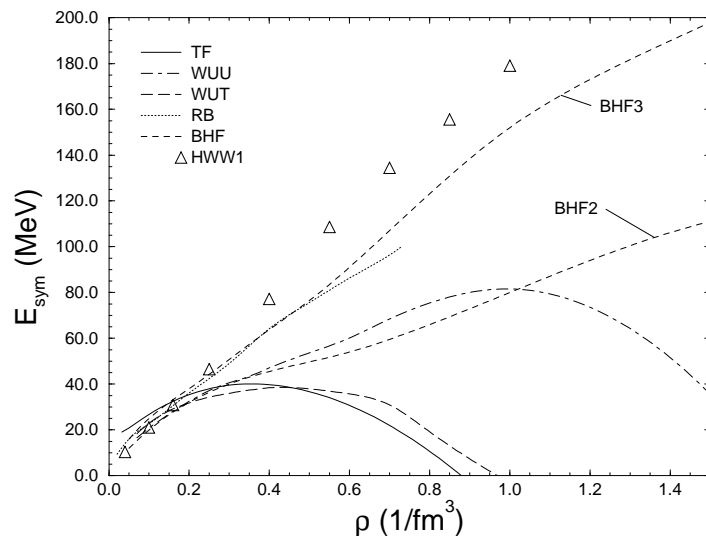


FIGURE 5

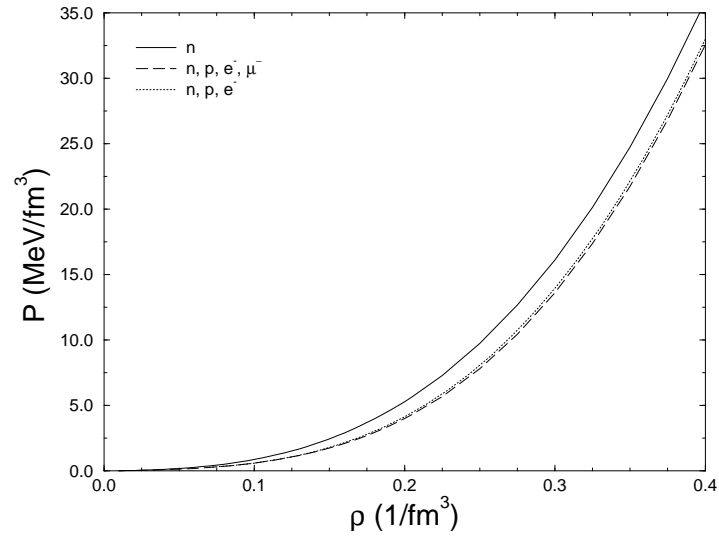


FIGURE 6

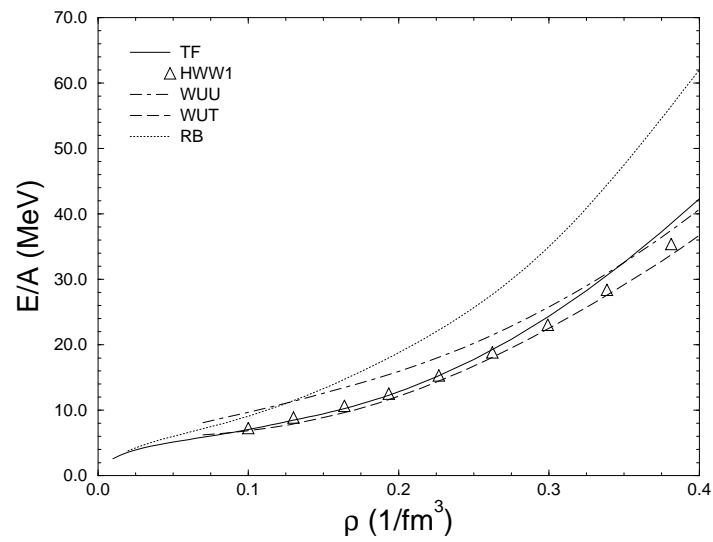


FIGURE 7

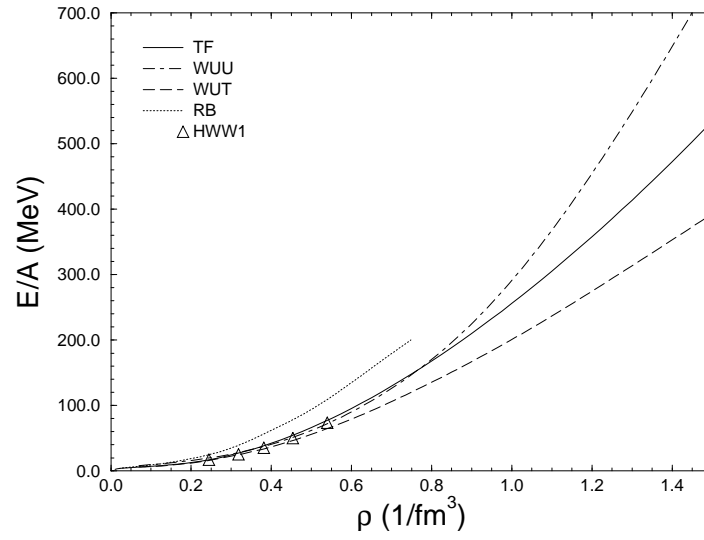


FIGURE 8

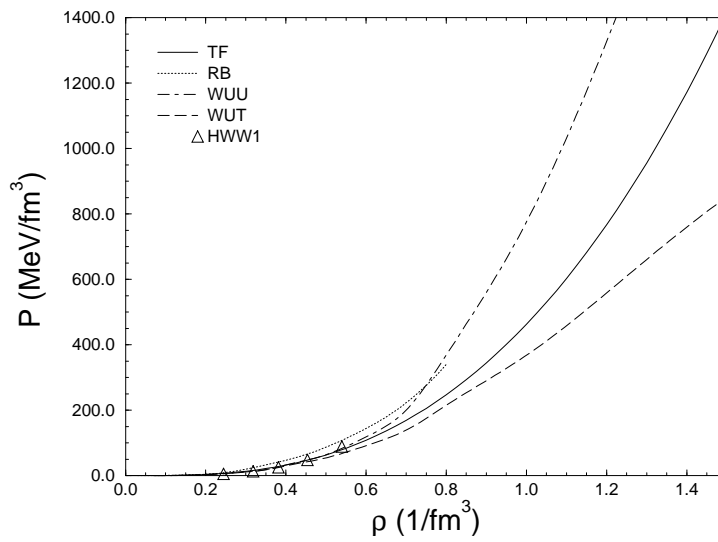


FIGURE 9

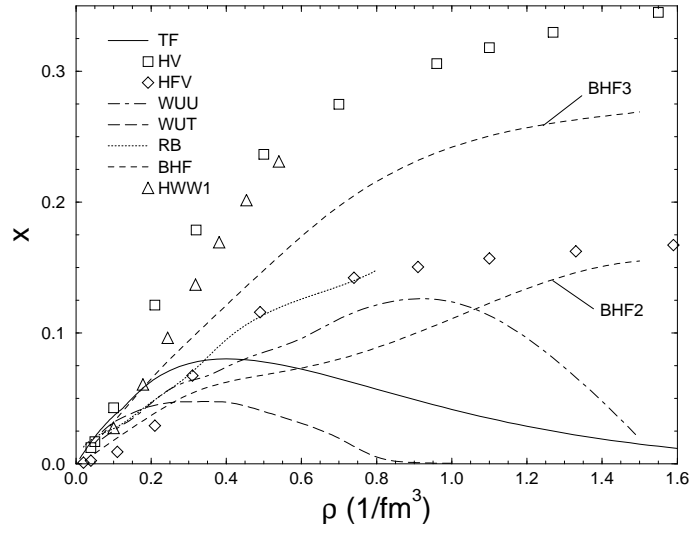


FIGURE 10

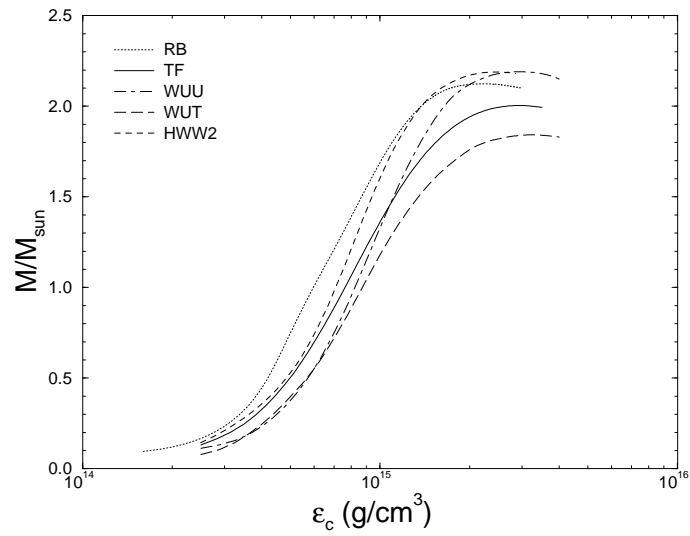


FIGURE 11

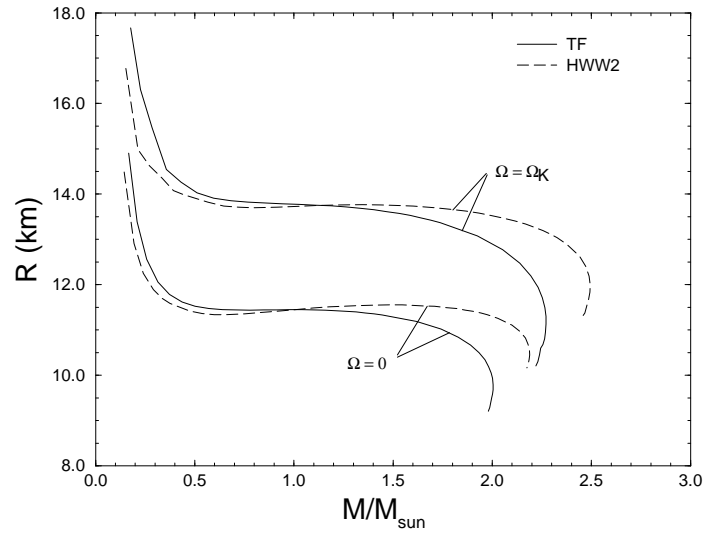


FIGURE 12

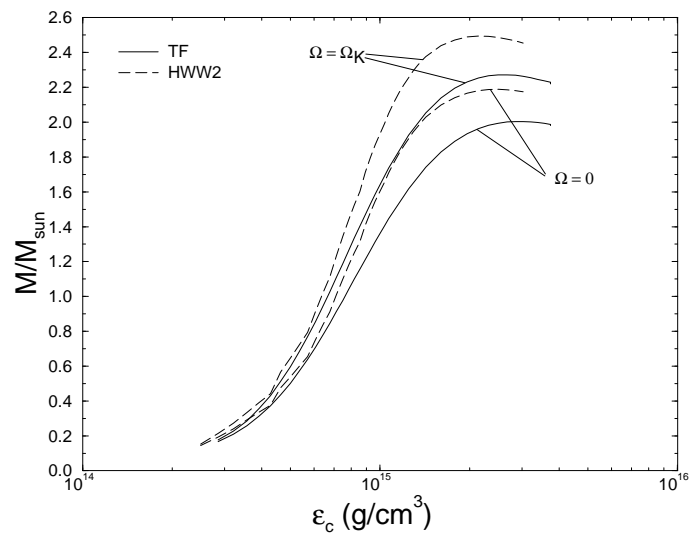


FIGURE 13

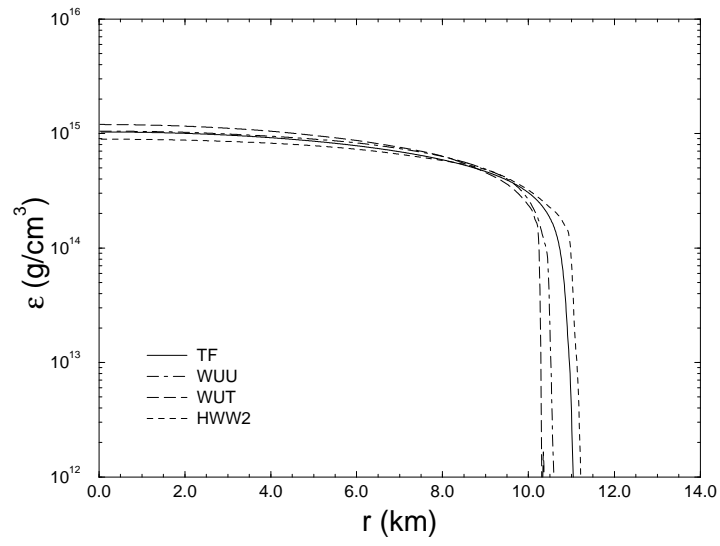


FIGURE 14

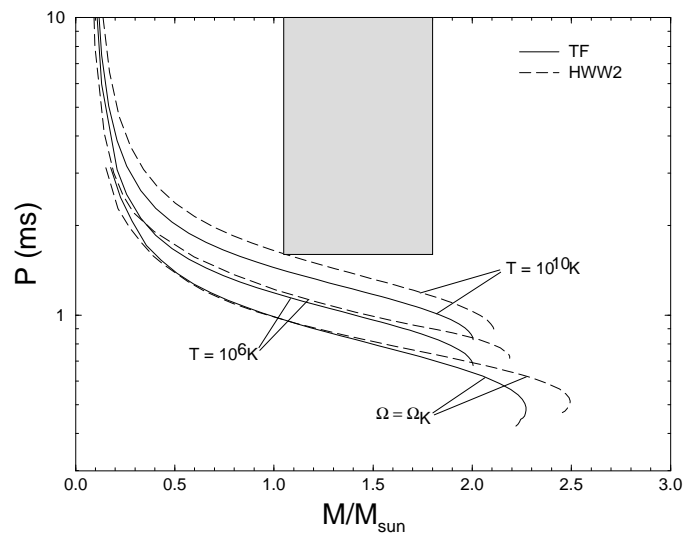
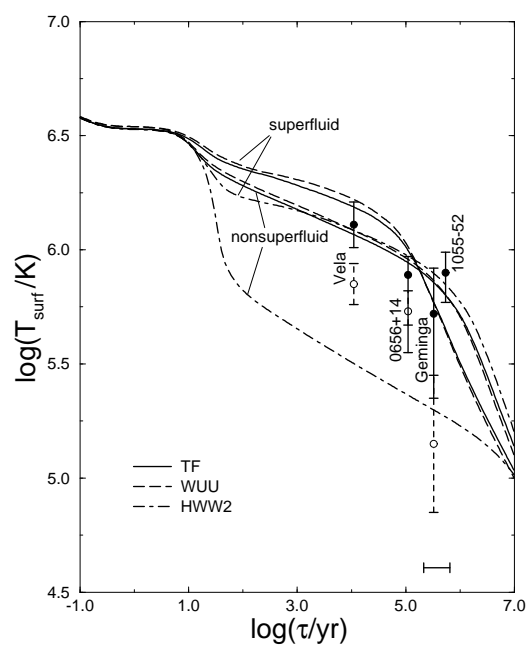


FIGURE 15



References

- [1] J. R. Oppenheimer and G. M. Volkoff, *Phys. Rev.* **55**, 374 (1939).
- [2] M. Ruderman, *Ann. Rev. Astron. Astrophys.* **10**, 472 (1972), and references therein.
- [3] F. Weber and N. K. Glendenning, in *Proceedings of the Nankai Summer School on Astrophysics and Neutrino Physics*, Tianjin, China, 1991, edited by D. H. Feng, G. Z. He, and X. Q. Li (World Scientific, Singapore, 1993) pp. 64–183, and references therein.
- [4] M. Prakash, I. Bombaci, M. Prakash, P. J. Ellis, J. M. Lattimer, and R. Knorren, *Composition and Structure of Protoneutron Stars*, preprint 1996 (nucl-th/9603042) and references therein.
- [5] G. E. Brown, in *Proceedings of the International Nuclear Physics Conference*, Beijing, China, 1995, edited by Sun Zuxun and Yu Jincheng (World Scientific, Singapore, 1996) pp. 623–634, and references therein.
- [6] D. Q. Lamb, J. M. Lattimer, C. J. Pethick, and D. G. Ravenhall, *Nucl. Phys.* **A360**, 459 (1981) and references therein.
- [7] J. M. Lattimer, C. J. Pethick, D. G. Ravenhall, and D. Q. Lamb, *Nucl. Phys.* **A432**, 646 (1985) and references therein.
- [8] R. B. Wiringa, V. Fiks, and A. Fabrocini, *Phys. Rev.* **C38**, 1010 (1988) and references therein.
- [9] M. Baldo, G. F. Burgio, and I. Bombaci, *Microscopic nuclear equation of state with three-body forces and neutron star structure*, preprint INFNCT 108–96, Catania, Italy and references therein.
- [10] W. D. Myers and W. J. Swiatecki, *Ann. of Phys.* **204**, 401 (1990); *Ann. of Phys.* **211**, 292 (1991) and references therein.
- [11] R. G. Seyler and C. H. Blanchard, *Phys. Rev.* **124**, 227 (1961); **131**, 355 (1963).
- [12] W. D. Myers and W. J. Swiatecki, *Ann. of Phys.* **55**, 395 (1969).

- [13] B. Friedmann and V. R. Pandharipande, Nucl. Phys. **A361**, 502 (1981).
- [14] D. Hartmann, M. F. El Eid, and M. Barranco, Astronomy and Astrophysics **131**, 249 (1984).
- [15] B. D. Serot and J. D. Walecka, Adv. Nucl. Phys. **16**, 1 (1986) and references therein.
- [16] B. D. Serot, Rep. Prog. Phys. **55**, 1855 (1992);
- [17] L. S. Celenza and C. M. Shakin, Relativistic Nuclear Physics (World Scientific, Singapore 1986), and references therein.
- [18] N. K. Glendenning, Astrophys. J. **293**, 470 (1985); Z. Phys. **A327**, 295 (1987), and references therein.
- [19] F. Weber and M. K. Weigel, Nucl. Phys. **A493**, 549 (1989); **A495**, 363c (1989); **A505**, 779 (1989).
- [20] P. Poschenrieder and M. K. Weigel, Phys. Lett. **B200**, 231 (1988); Phys. Rev. **C38**, 471 (1988).
- [21] H. Huber, F. Weber, and M. K. Weigel, Phys. Lett. **B317**, 485 (1993); Phys. Rev. **C51**, 1790 (1995), and references therein.
- [22] K. Strobel, Infinite Kern- und Neutronensternmaterie im Thomas-Fermi-Modell bei endlichen Temperaturen, Diploma thesis, Munich 1996.
- [23] W. D. Myers and W. J. Swiatecki, Nucl. Phys. **A601**, 141 (1996); The Nuclear Thomas-Fermi Model, LBL-Report - 36004 (1994); to be published in Proc. XXIX Zakopane School of Physics, Zakopane, Poland, 1994, in Acta Physica Polonica.
- [24] R. Brockmann and R. Machleidt, Phys. Rev. **C42**, 1965 (1990).
- [25] G. Q. Li, R. Machleidt, and R. Brockmann, Phys. Rev. **C45**, 2782 (1992).
- [26] K. Sumiyoshi, K. Oyamatsu, and H. Toki, Nucl. Phys. **A595**, 327 (1995).

- [27] H. Huber, F. Weber, and M. K. Weigel, *Phys. Rev.* **C50**, R1287 (1994).
- [28] H. Huber, F. Weber, and M. K. Weigel, An improved parametrization of RBHF-calculation, preprint, Munich 1996.
- [29] J. Boguta, *Phys. Lett.* **106B**, 255 (1981).
- [30] J. M. Lattimer, C. J. Pethick, M. Prakash, and P. Haensel, *Phys. Rev. Lett.* **66**, 2701 (1991).
- [31] H. Huber, F. Weber, and M. K. Weigel, *Nucl. Phys.* **A596**, 684 (1996).
- [32] J. L. Friedman, J. R. Ipser, and L. Parker, *Astrophys. J.* **304**, 115 (1986); *Phys. Rev. Lett.* **62**, 3015 (1989).
- [33] F. Weber and N. K. Glendenning, *Astrophys. J.* **390**, 541 (1992).
- [34] F. Weber, N. K. Glendenning, and M. K. Weigel, *Astrophys. J.* **373**, 579 (1991); in *Proceedings of the Second International Conference of Medium- und High-Energy Nuclear Physics*, Taipei, Taiwan, 1990, edited by W.-Y.P. Hwang et al. (North-Holland, New York, 1991).
- [35] Ch. Schaab, F. Weber, M. K. Weigel, and N. K. Glendenning, *Nucl. Phys.* **A605**, 531 (1996).
- [36] F. Weber and N. K. Glendenning, in *Proceedings of the First Symposium on Nuclear Physics in the Universe*, Oak Ridge, TN, 1992, edited by M. W. Guidry and M. R. Strayer (IOP, Bristol, UK, 1993), p. 127.
- [37] F. Nagase, *Publ. Astron. Soc.* **41**, 1 (1989).
- [38] Ch. Schaab, D. Voskresensky, A. D. Sedrakian, F. Weber, and M. K. Weigel, Impact of medium effects on the cooling of non-superfluid and superfluid neutron stars, to appear in *Astronomy and Astrophysics* (1996).
- [39] Ch. Schaab, B. Hermann, F. Weber, and M. K. Weigel, Differences of the Cooling Behavior of Strange Quark Matter Stars and Neutron Stars, *subm. to Phys. Rev. Letter* (1996).

- [40] K. A. Van Riper, B. Link, and R. I. Epstein, *Astrophys. J.* **448**, 294 (1995).
- [41] Ch. Schaab, A. D. Sedrakian, F. Weber, and M. K. Weigel, *Internal Heating and Evolution of Neutron Stars*, in preparation (1996).
- [42] G. G. Pavlov, V. E. Zavlin, J. Trümper, and R. Neuhäuser, *Multiwavelength Observations of Isolated Neutron Stars as a Tool to Probe the Properties of their Surfaces*, to be published in *Astrophys. J. Letters*.
- [43] M. Brack, C. Guet, and H.-B. Håkansson, *Phys. Rep.* **123**, 275 (1985).